J Mater Sci (2011) 46:6323–6331
DOI 10.1007/s10853-010-4937-y

ABBASCHIAN FESTSCHRIFT

# A study on the synthesis of nanostructured WC–10 wt% Co particles from $WO_3$, $Co_3O_4$, and graphite

**Y. Zhong · L. Shaw**

Received: 21 June 2010 / Accepted: 17 September 2010 / Published online: 30 October 2010


**Abstract** The formation of the nanostructured WC–10 wt% Co powder from $WO_3$, $Co_3O_4$, and graphite is studied. The effects of the processing parameters of high-energy ball milling, reduction in $H_2$ atmosphere, and carburization in Ar/CO atmosphere are investigated. The crystallite size of the as-synthesized WC is 30–40 and 40–50 nm for 900 and 1000 °C carburized powders, respectively. The powder is agglomerated with the size of the primary particles ranging from 50 to 700 nm. High-energy ball milling of $WO_3$–$Co_3O_4$–C powder mixtures leads to finer particle and crystallite sizes with larger surface area. Such milled powders can be reduced to nanostructured W at 570 °C and carburized to form WC at temperatures as low as 900 °C. Crystal growth has taken place during carburization, particularly at 1000 °C, which results in the formation of truncated triangular prisms and nanoplates of WC at 1000 °C.

## Introduction

Nanostructured materials have long been recognized to have remarkable and technologically attractive properties due to their fine microstructures [1]. Tungsten carbide–cobalt (WC–Co) cermet materials are widely used for a variety of applications, particularly in machining, cutting, and drilling. Cemented tungsten carbide with nanocrystalline grain structure has the potential to dramatically improve the mechanical properties of these materials [2]. Extensive effort has been put into the synthesis of nanostructured WC–Co powders in the last two decades, including ball milling [3–5], spray conversion process [6–10], and chemical vapor phase reaction [11–14]. A method integrating mechanical and thermal activations of $WO_3$, $Co_3O_4$, and graphite has been reported to be effective in synthesizing the nanostructured WC–18 wt% Co powder [15]. The basic form of the process is to mechanically activate reactants (usually a mixture of oxide and graphite powder) at room temperature through high-energy ball milling (the mechanical activation step), followed by completing the synthesis reaction at high temperatures (the thermal activation step) [15].

In spite of the success of the integrated mechanical and thermal activation (IMTA) process in making WC–18 wt% Co [15], other WC–Co compositions, particularly those with low Co concentrations (e.g., 6, 10, and 12 wt% Co) which have widespread industrial applications, have not been demonstrated. Such a concern arises because it has been shown that the reduction temperature of cobalt oxide during the IMTA process is much lower than that of tungsten oxide and the Co formed can, in turn, catalyzes the reduction of tungsten oxide [16]. Thus, nanostructured WC–Co cermets containing low Co concentrations may or may not be effectively produced via the IMTA process because of less Co available to catalyze the reduction of tungsten oxide. This study is performed to address this concern by investigating the feasibility of forming nanostructured WC–10 wt% Co via the IMTA process. If successful, this work will have significant technological implications because of the widespread application of WC–Co cermets with low Co concentrations. In addition, we have further investigated the effects of different reduction temperatures and carburization atmospheres that have not been studied previously. A single-step reaction containing both reduction and carburization has also been

Y. Zhong · L. Shaw (✉)
Department of Chemical, Materials and Biomolecular Engineering, University of Connecticut, Storrs, CT 06269, USA
e-mail: leon.shaw@uconn.edu

investigated. As will be shown below, the present investigation has successfully demonstrated the efficacy of the IMTA process in synthesizing WC–10 wt% Co. This is the first study showing that the IMTA process is suitable for synthesizing WC–Co cermets with low Co concentrations that have widespread industrial applications.

## Experimental

$WO_3$ (99.8%) and $Co_3O_4$ (99.7%) purchased from Alfa Aesar and graphite (>99.99%) purchased from Aldrich were used as the starting materials. Because of the large particle sizes, the as-received graphite powder was high-energy ball milled at room temperature for 6 h before being mixed with $WO_3$ and $Co_3O_4$. These $WO_3$, C, and $Co_3O_4$ powders were mixed in a molar ratio of 1:2.4:0.123 to form a final product of WC + 10 wt% Co. The mixed powders were subsequently ball milled using a modified Szegvari attritor, which has been shown to be effective in synthesizing a uniform milling product within the powder charge [15–18]. Tungsten carbide balls (WC with 5 wt% Co) of 4.76 mm in diameter were used as the milling media and mixed with powder at a ball-to-powder weight ratio of 60:1. The charged canister was evacuated up to $10^{-2}$ torr, flushed with argon, followed by evacuation and then being back filled with argon of purity 99.95% at a pressure of about 1.5 atm before the onset of milling. The canister was cooled with circulation water (20 °C) at a flow rate of about 770 mL/min throughout the entire process. A milling speed of 600 rpm and milling time of 6 h were employed for all the samples.

The ball milled powders were then subjected to reduction and carburization in a tube furnace to form nanostructured WC–Co powders. The reduction reaction was carried out by heating the milled powder at 570, 620, or 670 °C for 2 h in a mixture of $H_2$ ($P_{H_2} = 0.5$ atm) and Ar ($P_{Ar} = 0.5$ atm). After reduction, the powder was carburized at 1000 °C in either Ar ($P_{Ar} = 1.0$ atm) or CO ($P_{CO} = 1$ atm) atmosphere for 1 h. A single-step reaction combining both reduction and carburization was also investigated. In this case the powder was heated to 900 °C in CO ($P_{CO} = 1$ atm) for 2 h to form WC–Co powder directly. In order to identify the reaction pathways of reduction and carburization, the effluent gas from the tube furnace was constantly monitored using a quadrupole residual gas analyzer (RGA) equipped with a mass spectrometer (Model ppt-c300-F2Y). The gaseous species monitored by the RGA included $H_2$, $N_2$, $O_2$, $H_2O$, $CH_4$, $CO_2$, CO, and Ar.

The morphology of the as-milled and reacted powders and their sizes were characterized with the aid of a field-emission scanning electron microscope (FESEM, JEOL, JSM 6335F). Observations using a transmission electron microscope (TEM, JEOL, JSM 1230) were also performed. Phase identification was carried out by employing X-ray diffraction (XRD) with Cu Kα radiation (Bruker Axs D5005D X-ray Diffractometer). The average grain sizes of the powder were estimated based on XRD peak broadening using the Scherrer formula [19–22]. The carbon content in the WC–Co powder was determined using a combustion analyzer, Elementar (Elementar Analysensysteme, Germany).

## Results and discussion

Figure 1 shows SEM images of graphite before and after high-energy ball milling alone for 6 h. Graphite before ball milling has a flake morphology with a dimension of approximately $1 \times 10 \times 10$ μm$^3$. After 6 h of ball milling, graphite particles become round and their average sizes have been reduced to approximately 1–5 μm in diameter. The ball milled graphite with reduced sizes can be mixed with $WO_3$ and $Co_3O_4$ more uniformly. Figure 2 shows XRD patterns of graphite before and after ball milling, the pattern clearly revealed the graphite becomes amorphous or nanocrystalline after 6 h of ball milling. Figure 3 shows XRD patterns of the as-received $WO_3$ and $Co_3O_4$ powder as well as the $WO_3$–$Co_3O_4$–C powder mixtures after 2 and 6 h of ball milling. It can be seen that the starting $WO_3$ and $Co_3O_4$ powders are crystalline. The intensities of $WO_3$ peaks decrease with increasing the milling time. The substantial peak broadening induced by ball milling suggests the reduced crystallite size and/or the introduction of the internal strain. The crystallite size of $WO_3$ becomes 27 and 22 nm after 2 and 6 h of ball milling, respectively, based on the Scherrer formula. The absence of $Co_3O_4$ peaks in the mixture is most likely caused by a small amount of $Co_3O_4$ because a previous study [16] has revealed that even with 12 h of ball milling there is no formation of solid solutions between tungsten and cobalt oxides. Figure 4 shows the SEM images for $WO_3$–$Co_3O_4$–C after 2 and 6 h of ball milling. A comparison between Figs. 1 and 4 reveals that graphite particles have been further refined to around 2–3 μm after additional 2 h of ball milling. However, there is little change in the graphite particle size beyond this 2 h of ball milling, as shown in Fig. 4. It is also worth noting that the oxide particle size becomes submicron after ball milling, i.e., 30–200 nm after 2 h of milling and 20–150 nm after 6 h of milling. The XRD and SEM data clearly shows that the powder mixture after high-energy ball milling has ultrafine particle sizes with nanocrystallites and large specific areas. These features will significantly enhance the reaction kinetics via the increased reaction area and possibly the improved diffusivity.

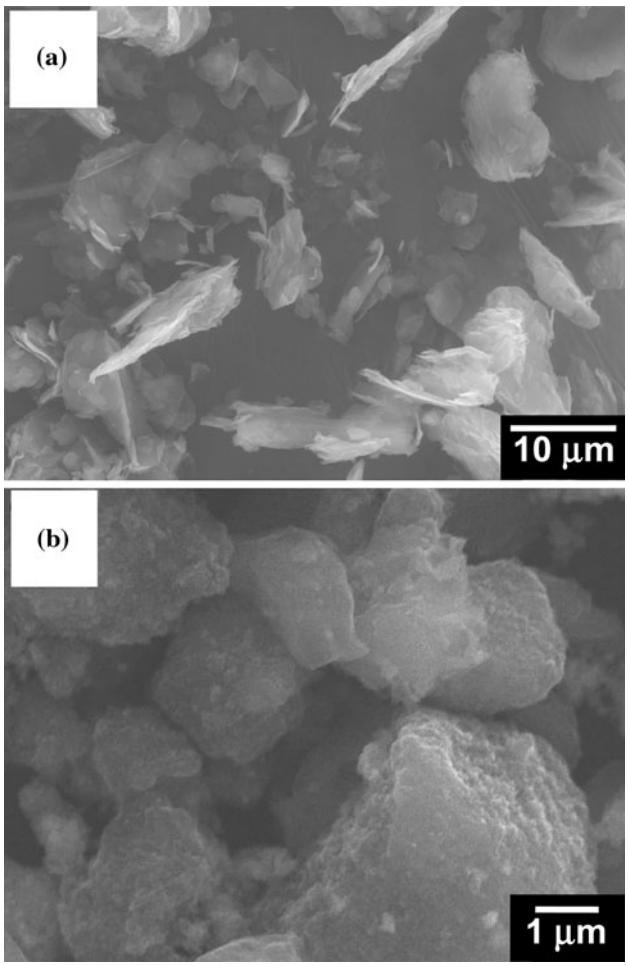


**Fig. 1** SEM images of graphite: **a** before and **b** after ball milling alone for 6 h

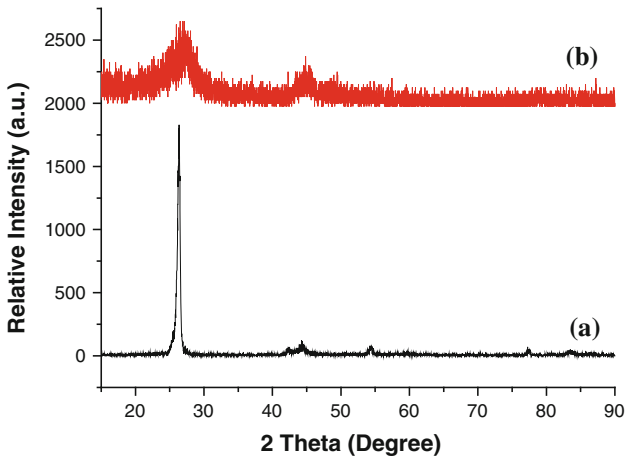


**Fig. 2** XRD patterns of graphite: (*a*) before and (*b*) after ball milling alone for 6 h

The synthesis of WC–Co powder from the milled $WO_3$–$Co_3O_4$–C mixture consists of two major steps: the reduction of $WO_3$ to W and the carburization of the reduced

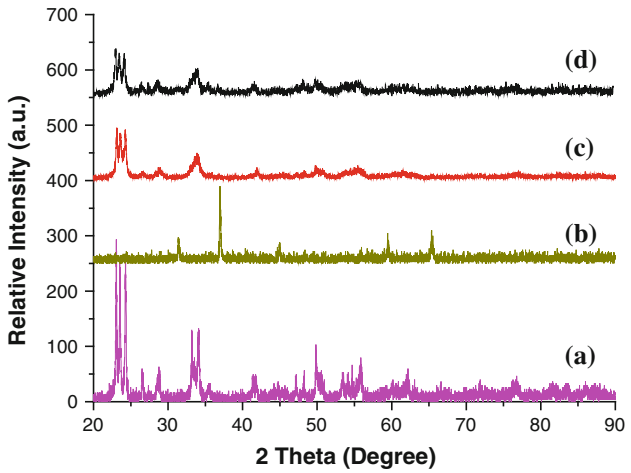


**Fig. 3** XRD patterns: (*a*) the as-received $WO_3$, (*b*) the as-received $Co_3O_4$, (*c*) the as-milled $WO_3$–$Co_3O_4$–C for 2 h, and (*d*) the as-milled $WO_3$–$Co_3O_4$–C for 6 h

powder. It has been reported that $WO_3$ can be reduced by $H_2$ [15, 16] and graphite [23]. Figure 5 shows the XRD patterns for the $WO_3$–$Co_3O_4$–C mixture after 2 or 6 h of milling and reduction in a $H_2$/Ar mixture at different temperatures. The XRD patterns indicate that $WO_3$ has been reduced to W at the considered temperatures (570, 620, and 670 °C), which are lower than the reduction temperature for making coarse-grained WC [24] and nanostructured WC [15, 16, 23]. In particular, the reduction temperatures achieved in this study are substantially lower than 900 °C used to reduce $WO_3$ when the reduction relies only on the carbon in the powder mixture even with 20 h of ball milling time [23]. Low reduction temperatures are highly desired because the average crystallite size of W increases with the reduction temperature, as shown in Fig. 6. The average crystallite size of W also decreases with increasing the milling time (Fig. 6). These trends are ascribed to grain growth during reduction and finer starting oxide particles, respectively. The average crystallite sizes estimated from XRD peak broadening have been corroborated by bright-field and dark-field TEM images of the 6 h milled $WO_3$–$Co_3O_4$–C mixture after being reduced at 670 °C (Fig. 7). The average grain sizes measured from TEM are around 15–20 nm, consistent with the XRD analysis (Fig. 6).

Another interesting finding from the XRD analysis (Fig. 5) is that $Co_3W$ has been formed in the reduction stage at 570 °C, and co-exists with $Co_6W_6C$ at higher temperatures (620 and 670 °C), which is in agreement with the finding of Ban and Shaw [16]. It can also be seen that as the $Co_6W_6C$ peak becomes stronger, the $Co_3W$ peak becomes weaker, suggesting the carburization of $Co_3W$ to form $Co_6W_6C$ as temperature increases. Furthermore, the powder mixtures with 6 h of ball milling exhibit more

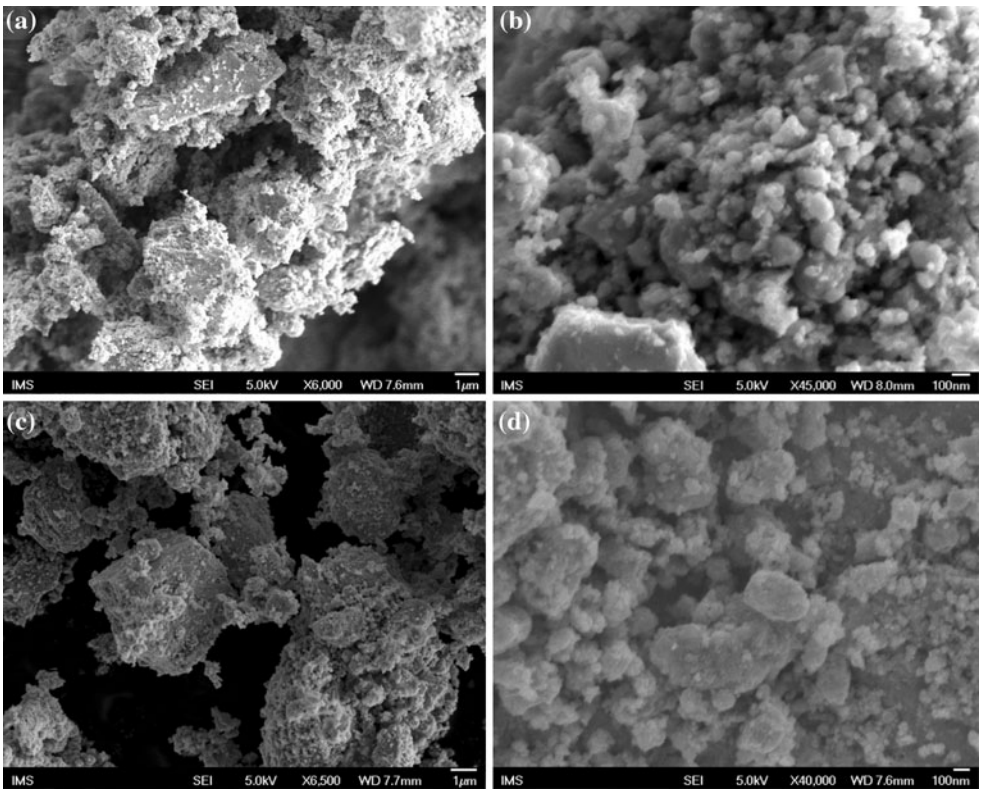


**Fig. 4** SEM images of $WO_3 + Co_3O_4 + C$ powder mixtures: **a**, **b** ball milled for 2 h, and **c**, **d** ball milled for 6 h

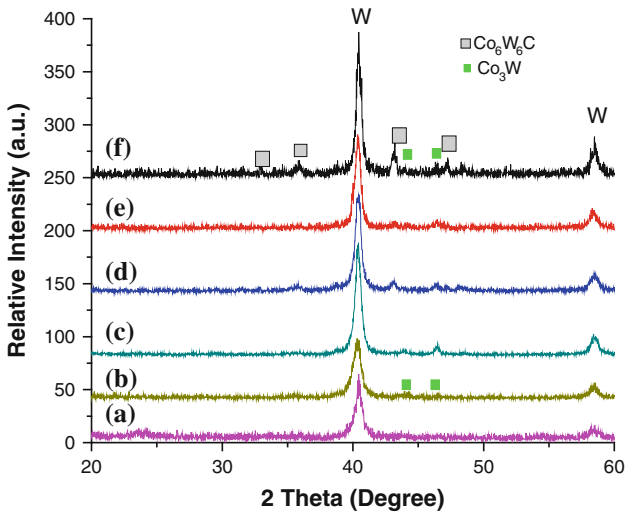


**Fig. 5** XRD patterns of ball milled $WO_3 + Co_3O_4 + C$ mixtures after reduction in an $Ar/H_2$ atmosphere with the ball milling time and reduction temperature as: (*a*) 2 h milling, 570 °C; (*b*) 6 h milling, 570 °C; (*c*) 2 h milling, 620 °C; (*d*) 6 h milling, 620 °C; (*e*) 2 h milling, 670 °C; and (*f*) 6 h milling, 670 °C

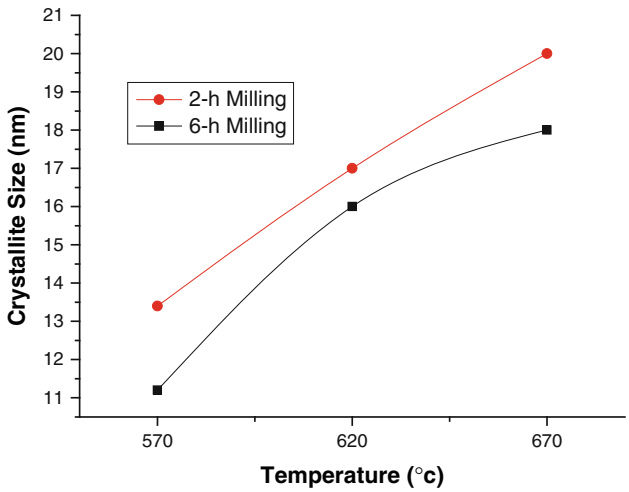


**Fig. 6** Average crystallite sizes for W after reduction reactions

$Co_3W$ and $Co_6W_6C$ formation than the counterparts with 2 h of ball milling, indicating that the reaction kinetics have been enhanced by ball milling. The Co peaks, however, are not observed at these temperatures. Since cobalt oxides can be reduced to Co at 450 °C [16], the absence of the Co peaks is likely due to the fast reaction of Co with W to form $Co_3W$.

Figure 8 shows the SEM images of the $WO_3$–$Co_3O_4$–C mixture with different milling times and after reduction at different temperatures. The particle sizes display the same trend as the crystallite sizes, i.e., increasing with the reduction temperature and decreasing with the milling

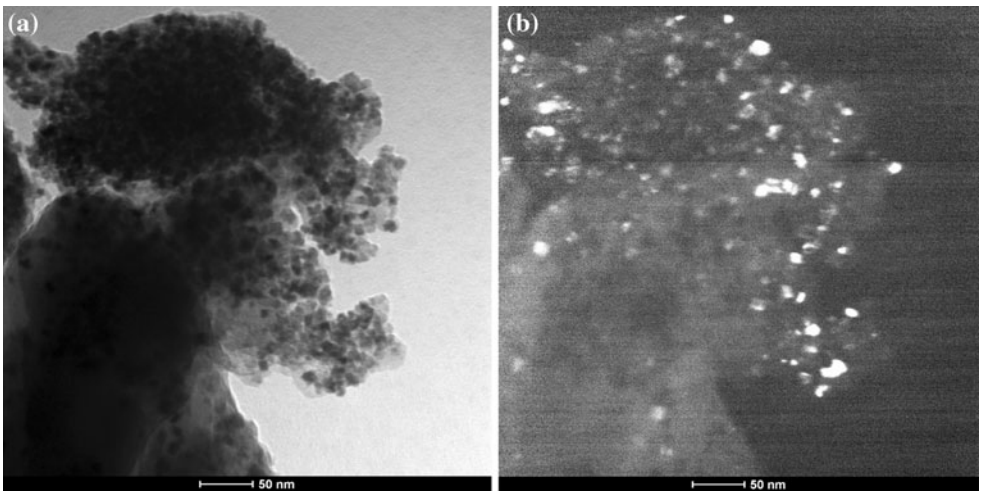


**Fig. 7** **a** Bright-field and **b** dark-field TEM images for the $WO_3 + Co_3O_4 + C$ powder mixture after 6 h of milling and reduced at 670 °C for 2 h

time. The powder appears to be agglomerated, while the primary particles forming these agglomerates have sizes ranging from 30 to 50 nm. These nanostructured W, $Co_3W$, and $Co_6W_6C$ powder mixtures with particle sizes of 30–50 nm and grain sizes in the range of 15–20 nm are the starting materials for the carburization stage.

To further identify the reaction pathways during the reduction stage, analysis of the effluent gas from the tube furnace based on mass spectrometry has been performed. Several interesting features can be identified from the gas profile shown in Fig. 9. First, the dramatic change in most of the gases takes place in the first half an hour of the reduction at 670 °C, indicating that most reactions occur at this time period. Second, the intensities of CO, $CO_2$, $H_2O$, and $CH_4$ increase substantially when the furnace reaches the reaction temperature of 670 °C. Third, the intensity of $H_2$ decreases continuously in the reduction stage. These phenomena suggest that the oxide particles are reduced by both graphite and $H_2$. Furthermore, $H_2$ also reacts with graphite to form $CH_4$ during the reduction stage. Reactions (1) to (9) listed all the reactions in the reduction stage at 670 °C based on the RGA and XRD analyses.

$$WO_3 + 3C = W + 3CO \quad (1)$$

$$2WO_3 + 3C = 2W + 3CO_2 \quad (2)$$

$$WO_3 + 3H_2 = W + 3H_2O \quad (3)$$

$$Co_3O_4 + 4C = 3Co + 4CO \quad (4)$$

$$Co_3O_4 + 2C = 3Co + 2CO_2 \quad (5)$$

$$Co_3O_4 + 4H_2 = 3Co + 4H_2O \quad (6)$$

$$C + 2H_2 = CH_4 \quad (7)$$

$$3Co + W = Co_3W \quad (8)$$

$$2Co_3W + 4W + C = Co_6W_6C \quad (9)$$

The total carbon amount for the 6 h milled $WO_3$–$Co_3O_4$–C before and after reduction at different temperatures was measured using the Elementar instrument. The loss of carbon amount in the sample after reduction at 570, 620, and 670 °C is shown in Fig. 10. Reduction at 570 °C has the smallest carbon loss (~30%) because of the slow kinetics of forming $CH_4$. However, reduction at 620 °C leads to more carbon loss (~45%) than at 670 °C (~40%) because of the higher thermodynamic driving force at 620 °C [25]. Based on the analyses above, it is concluded that a large amount of $Co_6W_6C$ is formed with a relatively low loss of carbon at 670 °C for the 6 h milled powder mixture. Since the presence of $Co_6W_6C$ and C can expedite the formation of WC in the carburization stage [16], reduction at 670 °C for the 6 h milled powder mixture is further studied for the carburization reaction.

The as-reduced powder is held at 1000 °C for 1 h in a pure Ar ($P_{Ar} = 1$ atm) or CO ($P_{CO} = 1$ atm) atmosphere. The XRD patterns for the powder mixture after holding at 1000 °C for 1 h in Ar and CO, respectively, are shown in Fig. 11a and b. A single-step reaction combining simultaneous reduction and carburization is also studied. In this case the as-milled powder mixture is directly heated up to 900 °C and held at that temperature for 2 h in a CO atmosphere ($P_{CO} = 1$ atm). Figure 11c shows the XRD pattern for the 6 h milled powder mixture after the single-step reaction. Several distinctive features are noted for these XRD patterns. First, the patterns clearly show that WC and Co have formed during the carburization reactions for all the samples. The formation of WC at 900 °C is substantially lower than the temperatures reported previously in forming WC. The typical carburization

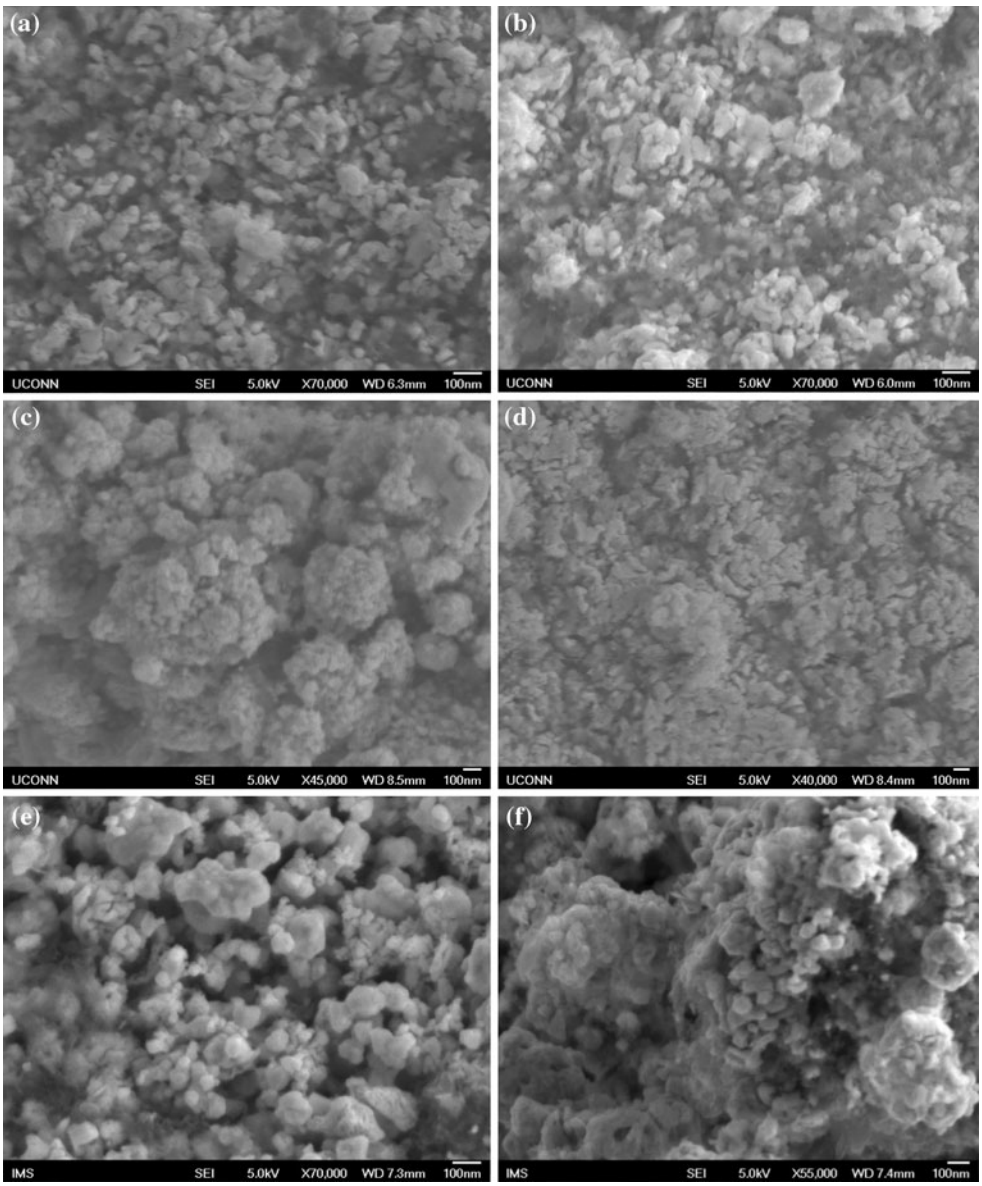


**Fig. 8** SEM images of $WO_3 + Co_3O_4 + C$ powder mixtures after ball milling and reduction in an $Ar/H_2$ atmosphere with the milling time and reduction temperature as: **a** 2 h milling, 570 °C; **b** 6 h milling, 570 °C; **c** 2 h milling, 620 °C; **d** 6 h milling, 620 °C; **e** 2 h milling, 670 °C; and **f** 6 h milling, 670 °C

temperature in the conventional process for making coarse-grained WC–Co is in the range of 1400–1600 °C [26]. Second, $CoC_x$ peaks are found in patterns (a) and (c). Note that $CoC_x$ is a metastable phase and has only been reported as a product of spray coating or laser sintering of WC–Co [27–29]. The $CoC_x$ found in this study is believed to be formed by the diffusion of the nanoscale carbon into the Co phase during the carburization reaction. The over-saturated Co phase due to the capillary effect of the nanoscale carbon particles retains sufficient carbon during the cooling process and forms the metastable $CoC_x$ phase at room temperature. Third, the $CoC_x$/Co peaks in the pattern of the single-step reaction product are much stronger compared with the two-step reactions. In the two-step reaction Co reacts with W to form $Co_3W$ which is subsequently carbonized to form $Co_6W_6C$ during the reduction stage. The $Co_6W_6C$ eventually becomes WC at the carburization stage, rejecting Co from the carbide phase. In the single-step reaction, the reduction of $WO_3$ and the carburization of W can take place sequentially without engaging the formation of $Co_3W$. As such, Co does not go through dissolution and rejection processes and thus WC particles are likely mixed with $Co/CoC_x$ particles physically. The different pathways in forming $Co/CoC_x$ phases in the single- and two-step reactions are presumably the sources for different intensities of $Co/CoC_x$ peaks in different samples.

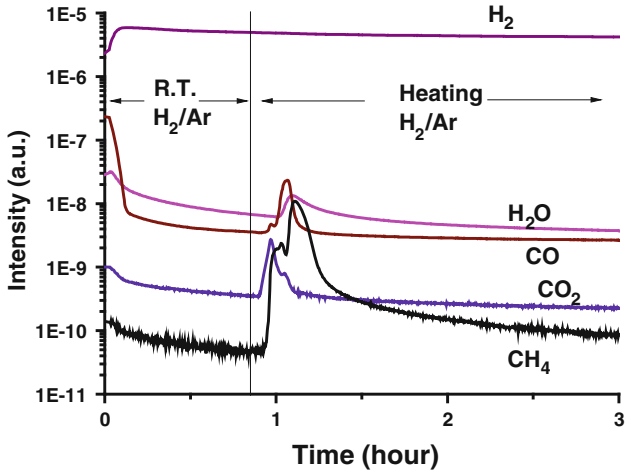


**Fig. 9** The composition profile of the effluent gas from the tube furnace during reduction. The sample was held inside the furnace at room temperature for 50 min with flowing argon ($P_{Ar} = 0.5$ atm) and hydrogen ($P_{H_2} = 0.5$ atm) before the onset of heating. The furnace was heated to 670 °C in about 10 min and held at that temperature for 2 h

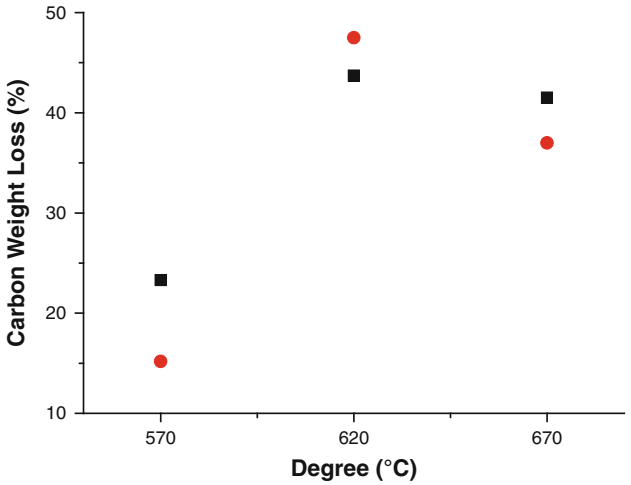


**Fig. 10** Carbon weight loss for the 6 h ball milled $WO_3 + Co_3O_4 + C$ mixture after reduction at different temperatures (570, 620, and 670 °C) for 2 h. Each reduction experiment has been repeated once to ensure the accuracy of the trend

However, the precise mechanism remains to be investigated.

The crystallite size of WC along different crystallographic directions based on the XRD peak broadening and Scherrer formula is shown in Table 1. The crystallite sizes are 40–50 nm for the two-step reactions, whereas they are in the range of 30–40 nm for the single-step reaction. The difference is likely due to the temperature effect with the two-step reaction at 1000 °C and the single-step reaction at 900 °C. It is also noted that the crystallite sizes along different crystallographic directions are similar for all the powders synthesized in this work, suggesting that WC

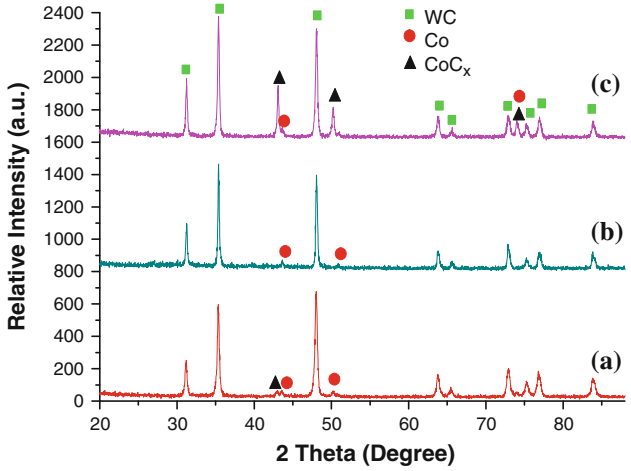


**Fig. 11** XRD patterns of (*a*) the 6 h ball milled mixture after reduction at 670 °C and carburization at 1000 °C for 1 h in Ar, (*b*) the 6 h ball milled mixture after reduction at 670 °C and carburization at 1000 °C for 1 h in CO, and (*c*) the 6 h ball milled mixture after reduction and carburization at 900 °C for 2 h in CO

**Table 1** Estimated crystallite sizes along $\langle 0001 \rangle$, $\langle 10\bar{1}0 \rangle$, and $\langle 10\bar{1}1 \rangle$ of WC particles synthesized by different methods

| | $\langle 0001 \rangle$ | $\langle 10\bar{1}0 \rangle$ | $\langle 10\bar{1}1 \rangle$ |
|---|---|---|---|
| Reduction at 670 °C in $H_2$/Ar | 46 nm | 48 nm | 41 nm |
| Carburization at 1000 °C in Ar | | | |
| Reduction at 670 °C in $H_2$/Ar | 47 nm | 58 nm | 46 nm |
| Carburization at 1000 °C in CO | | | |
| Reduction and carburization at 900 °C in CO | 38 nm | 32 nm | 40 nm |

grains are equiaxied. The morphologies of the WC–Co powders obtained are shown in Fig. 12. Agglomeration is clearly visible, and the sizes of the primary particles forming the agglomerates range from 50 nm to as large as 700 nm for all the powders. However, the particles carburized at 1000 °C exhibit facets, while the particles carburized at 900 °C show little faceting. The absence of facets in the 900 °C processed sample indicates that powder particles have not grown anisotropically at 900 °C. In contrast, the powder particles carburized at 1000 °C have undergone some anisotropic crystal growth in preferred directions. These observations are consistent with the trend shown by the estimation of the WC crystallite sizes (Table 1).

Finally, it is interesting to note that the faceted particles display several morphologies including truncated triangular prisms and nanoplates. It is established that WC has a HCP crystal structure with two sets of three equivalent $(10\bar{1}0)$ planes rather than six equivalent $(10\bar{1}0)$ planes [30]. Because of this unique nature of the crystal structure, WC

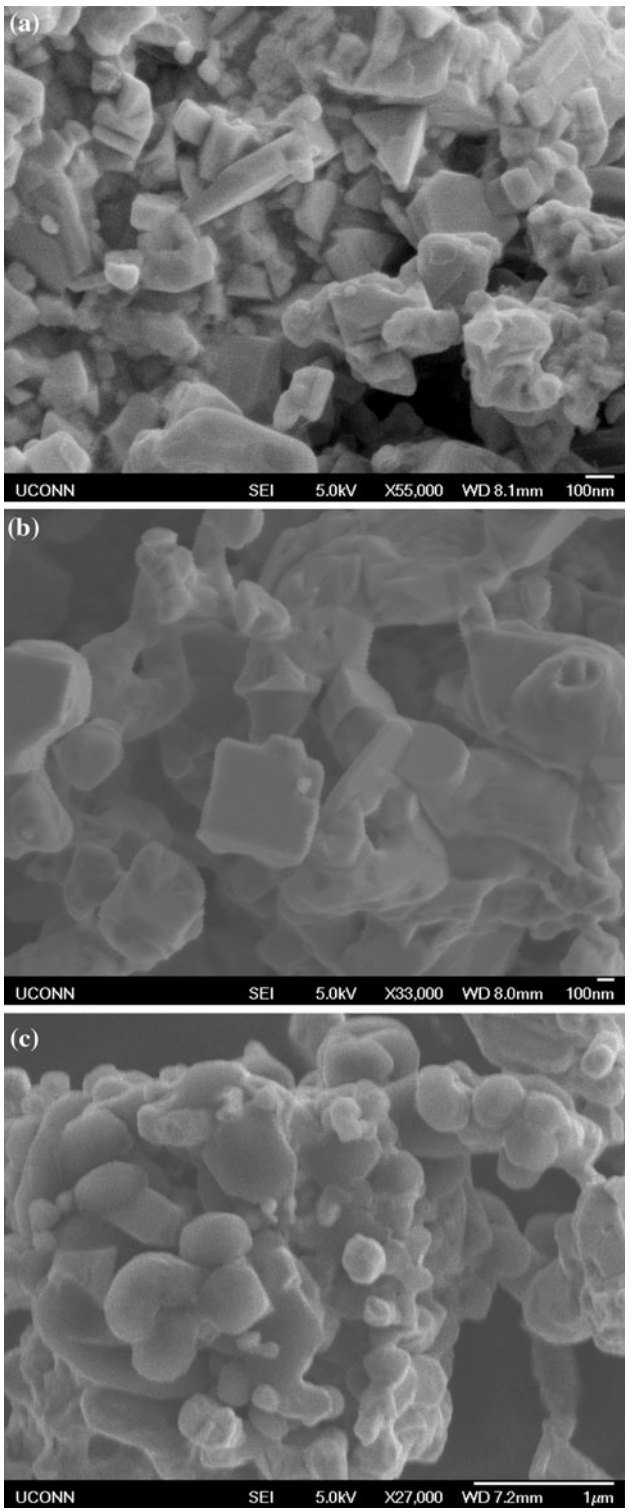


**Fig. 12** SEM images of 6 h ball milled $WO_3 + Co_3O_4 + C$ mixtures after reduction at 670 °C for 2 h and then carburization at 1000 °C for 1 h in **a** Ar, **b** CO, and **c** after single-step reduction and carburization at 900 °C for 2 h

crystals grown from liquid metal solutions assume the morphology of truncated triangular prisms [31, 32]. Such a prismatic shape has also been observed in fully sintered WC–Co cermets [30]. Thus, the formation of faceted particles is consistent with the crystal structure of WC. However, this study reports the lowest temperature in forming truncated triangular prisms and nanoplates of WC in comparison with the data in the open literature [30–32].

## Concluding remarks

A systematic study has been conducted on the synthesis of nanostructured WC–Co particles from $WO_3$, $Co_3O_4$, and graphite. The feasibility of using the IMTA process to synthesize nanostructured WC–Co powder with low Co concentrations, such as WC–10 wt% Co, has been demonstrated for the first time. The crystallite size of the as-synthesized WC is 30–40 and 40–50 nm for 900 and 1000 °C carburized powders, respectively. The powder is agglomerated with the size of the primary particles ranging from 50 to 700 nm. High-energy ball milling of $WO_3$–$Co_3O_4$–C powder mixtures leads to finer particle and crystallite sizes with larger surface area. Such milled powders can be reduced to nanostructured W at 570 °C and carburized to form WC at temperatures as low as 900 °C. The crystallite size of W (15–20 nm) is found to increase with the reduction temperature and decreases with increasing the milling time. The formation of WC proceeds with the formation of intermediates, $Co_3W$ and $Co_6W_6C$. Grain growth has taken place during the carburization stage, as indicated by the crystallite size of W (15–20 nm) becoming 30–40 or 40–50 nm for the crystallite size of WC carburized at 900 and 1000 °C, respectively. Crystal growth at 1000 °C is particularly obvious with the formation of truncated triangular prisms and nanoplates of WC, whereas only limited crystal growth occurs at 900 °C with WC particles showing no clear facets.

**Acknowledgements** This research was sponsored by the U.S. National Science Foundation (NSF) under the contract number CMMI-0856122. The support and vision of Dr. Mary Toney is greatly appreciated.

## References

1. Gleiter H (1992) Nanostruct Mater 1:1
2. Fang Z, Wang X, Ryu T, Hwang K, Sohn H (2009) Int J Refract Metals Hard Mater 27:288
3. Porat R, Berger S, Rosen A (1996) Mater Sci Forum 629:225
4. Fecht HJ (1992) Nanostruct Mater 1:125
5. Fecht HJ, Hellstern E, Fu Z, Johnson WL (1990) Metall Mater Trans A 21:2333
6. Gao L, Kear BH, Seegopaul P (1999) US Patent 5,919,428
7. Seegopaul P, Gao L (2003) US Patent 6,524,366
8. Kim BK, Ha GG, Woo Y (2003) US Patent 6,511,551
9. Lee G, Ha GH, Kim BK (1999) J Korean Inst Metal Mater 37:1233

10. Zhang ZY, Wahlberg S, Wang MS, Muhammed M (1999) Nanostruct Mater 12:163
11. Ryu T, Sohn HY, Han G, Kim Y, Hwang KS, Mena M, Fang ZZ (2008) Metall Mater Trans B 39:1
12. Hojo J, Oku T, Kato A (1978) J Less-Common Metal 59:85
13. Fitzsimmons M, Sarin VK (1995) Surf Coat Technol 76:250
14. Kim JC, Kim BK (2004) Scripta Mater 50:969
15. Ban ZG, Shaw L (2002) J Mater Sci 37:3397. doi:10.1023/A:1016553426227
16. Ban ZG, Shaw L (2001) Acta Mater 49:2933
17. Yang ZG, Shaw L (1996) Nanostruct Mater 7:873
18. Zhong Y, Shaw L, Manjarres M, Zawrah MM (2010) J Am Ceram Soc 93:3159
19. Klug HP, Aexander LE (1974) X-ray diffraction procedures for polycrystalline and amorphous materials. Wiley, New York
20. Snyder RL, Fiala J, Bunge HJ (1999) Defect and microstructure analysis by diffraction. Oxford University Press, Oxford
21. Mittermeijer EJ, Scardi P (2004) Diffraction analysis of the microstructure of materials. Springer-Verlag, Berlin
22. Ungar T (2004) Scripta Mater 51:777
23. Liu W, Song X, Zhang J, Zhang G, Liu X (2008) Mater Chem Phys 109:235
24. Aronsson B, Pastor H (1991) Powder metallurgy: an overview. The Institute of Metals, London
25. Binnewies M, Milke E (2002) Thermochemical data of elements and compounds, 2nd edn. Wiley-VCH, Weinheim
26. Yih S, Wang C (1979) Tungsten: source metallurgy properties and applications. Plenum Press, New York, p 385
27. Gu D, Shen Y (2006) Mater Lett 60:3664
28. de Villiers HL (1998) J Therm Spray Technol 7:357
29. Sahraoui T, Guessasma S, Ali Jeridane M, Hadji M (2010) Mater Design 31:1431
30. Exner HE (1979) Int Mater Rev 24:149
31. French DN, Thomas DA (1968) In: Vahldiek FV, Mersol J (eds) Anisotropy in single-crystal refractory compounds, vol 1. Plenum Press, New York
32. Takahashi T, Freise EJ (1965) Philos Mag 12:1